Received: 29 July 2023 | Revised: 20 September 2023 | Accepted: 22 September 2023

DOI: 10.1111/jace.19506

Journal of the American Ceramic Society

RAPID COMMUNICATION

A simple synthetic approach to $BaZrS_3$, $BaHfS_3$, and their solid solutions

Lorenza Romagnoli[1] | **Andrea Ciccioli**[1] | **Phillip J. Dale**[2] | **Hasan Arif Yetkin**[2] | **Riccardo Panetta**[3] | **Alessandro Latini**[1]

[1]Dipartimento di Chimica, Sapienza Università di Roma, Roma, Italy

[2]Department of Physics and Materials Science, University of Luxembourg, Belvaux, Luxembourg

[3]Ispa - Istituto Sperimentale Problematiche Ambientali, Atina, Italy

Correspondence
Andrea Ciccioli, Dipartimento di Chimica, Sapienza Università di Roma, Piazzale Aldo Moro 5, 00185 Roma, Italy.
Email: andrea.ciccioli@uniroma1.it

Phillip J. Dale, Department of Physics and Materials Science, University of Luxembourg, L-4422 Belvaux, Luxembourg.
Email: phillip.dale@uni.lu

Alessandro Latini, Dipartimento di Chimica, Sapienza Università di Roma, Piazzale Aldo Moro 5, 00185 Roma, Italy.
Email: alessandro.latini@uniroma1.it

Funding information
Sapienza Università di Roma, Grant/Award Number: RM12117A8484C2E0

Abstract

A simple synthetic approach to $BaZrS_3$, $BaHfS_3$, and their solid solutions is presented and discussed here. The synthesis is performed under relatively mild conditions (T = 500°C) and is complete in a few hours. The reactants are powdered BaS, Me (Me: Zr, Hf) and S in a ratio 1:1:3, mixed and sealed under vacuum in borosilicate glass ampoules. No purification is usually required, and the yield is quantitative. The low synthesis temperature allows for the use of borosilicate glass as container material instead of silica glass, thus lowering the costs and simplifying the sealing of the reaction vessel; furthermore, the use of expensive ZrS_2 and HfS_2 is avoided. The same procedure was successfully used for the synthesis of solid solutions $BaHf_{1-x}Zr_xS_3$ that were always obtained as crystalline single-phase materials. The solid solutions display optical and structural properties that vary in a linear fashion with the composition and are intermediate between those of $BaZrS_3$ and $BaHfS_3$. The possibility of varying the band gap of the material between 1.78 ($BaZrS_3$) and 2.11 eV ($BaHfS_3$) in a continuous way by simply adjusting the Hf/Zr ratio is very intriguing for potential applications in multi-junction and in-door photovoltaic applications and light emitting devices.

KEYWORDS
ceramic semiconductors, chalcogenide perovskites, solid solutions, sulfide semiconductors

1 | INTRODUCTION

Inorganic chalcogenide perovskites such as $BaZrS_3$ and $BaHfS_3$ are attracting an increasing interest as semiconductor materials since they exhibit similar physical properties of hybrid metal halide perovskites (HMHPs), such as extraordinarily high light absorption coefficients and band gap values in the useful range for photovoltaic applications and most importantly high chemical and physical stability, typical of ceramic compounds.[1–6] Considering that the intrinsic instability of HMHPs[7–13] still prevents their use in real life devices, chalcogenide perovskites represent valid candidates that deserve to be thoroughly studied as alternative materials.

Despite the advantages that chalcogenide perovskites possess compared to HMHPs, they have also their drawbacks. The most relevant drawback is their challenging synthesis compared to HMHPs and the current lack of

simple and efficient methods for their deposition as thin films.[14,15]

Many synthetic approaches have been proposed for the synthesis of $BaZrS_3$ and/or $BaHfS_3$, such as:

- high temperature sulfurization of oxide and/or carbonate precursors with CS_2 or H_2S at high temperatures (700–1100°C)[16–18];
- the reaction of BaS and ZrS_2 in presence of excess sulfur with the addition of $BaCl_2$ as catalyst in the temperature range 450–600°C, with the perovskite always contaminated with variable amounts of ZrO_2, and in some cases by BaS_3 and ZrS_3[19,20];
- reaction of barium sulfide, zirconium, sulfur and iodine in the temperature range 600–1100°C for 60 h[21];
- solution phase syntheses using molecular precursors and/or metal hydrides of Zr and Hf dissolved in high boiling point solvents under strictly air and water-free conditons.[15,22]

All these methods present problems due to safety concerns (e.g., the use of highly poisonous and flammable CS_2 and H_2S), contaminations of the desired materials with undesired byproducts that cannot be easily removed, high synthesis temperatures that require the use of silica glass and expensive and difficult to manipulate reactants as well as strictly controlled reaction conditions.

The method presented in this work makes use of commercially available BaS, Zr/Hf and S powders in the molar ratio 1:1:3 BaS:Zr/Hf:S to easily obtain $BaZrS_3$, $BaHfS_3$, and $BaHf_{1-x}Zr_xS_3$ compounds.

2 | EXPERIMENTAL

2.1 | Materials preparation

2.1.1 | Materials

All the reactants were used as received without further purification. Barium sulfide powder (99.7%) was purchased from abcr. Zirconium powder 60–100 mesh (99.8% purity) was purchased from Chempur. Hafnium powder 325 mesh (99.5% purity excluding 2–4% Zr), sulfur powder (99.98% purity), toluene (ACS-ISO grade), Hf and Zr inductively coupled plasma-optical emission spectroscopy (ICP-OES) standards were purchased from Sigma Aldrich-Merck. Barium chloride (99%) was purchased from Carlo Erba and dried at 150°C for 2 h before use. Wheaton 10 mL prescored clear borosilicate glass ampules were purchased from Sigma Aldrich-Merck.

2.1.2 | Synthesis protocol

BaS, Zr(Hf), and S powders in molar ratio 1:1:3 (in case, with the addition of $BaCl_2$ with a $BaCl_2$/BaS molar ratio 1:10) were thoroughly mixed in an agate mortar in air for 20 min, then the powder mixture was transferred in a 10 mL glass ampule previously dried at 150°C for 30 min. The ampule was then connected to a rotary vane pump and evacuated to a pressure of approximately $3{\bullet}10^{-1}$ mbar. While connected to the vacuum pump, the ampule was heated to approximately 80°C with a hair dryer to remove any remaining moisture. After cooling to room temperature, the ampule, still connected to the operating vacuum pump, was flame sealed with a common mini butane torch. Once cooled to room temperature, the sealed ampule was inserted in a 100 mL alumina crucible, and then the crucible with the ampule was inserted in a muffle furnace preheated at 500°C and kept at the same temperature overnight. Then the crucible with the ampule is removed from the furnace still at 500°C and left at room temperature for natural cooling. The use of an alumina or porcelain crucible is essential to avoid an excessive thermal shock to the ampoule during its quenching to room temperature that would cause its breaking.

When cooled to room temperature, the ampule was opened and the solid recovered with a stainless steel spatula and grinded in an agate mortar. In case of elemental sulfur contamination of the product, it was stirred in hot toluene (85°C) for 1 h with a ratio of approximately 50 mL of toluene per gram of solid. The hot suspension was then filtered on paper under suction, washed three times with little amounts of toluene and kept under suction for drying for at least 1 h.

2.2 | Characterization

2.2.1 | Powder X-ray diffraction

Powder diffraction patterns acquisitions on the samples were performed with a Malvern Panalytical X'Pert Pro MPD diffractometer using the Cu Kα radiation ($\lambda = 1.54184$ Å). The scans were performed in the angular range 10–90° (in 2θ). The diffraction patterns were recorded using an ultrafast X'Celerator RTMS detector. The goniometer was calibrated with a factory polycrystalline Si standard. Rietveld refinement of the experimental diffraction patterns for the calculation of unit cell parameters of the compounds were performed using the MAUD software.

2.2.2 | UV-Vis spectroscopy

Diffuse reflectance UV-Vis spectra of the samples in the wavelength range 220–1400 nm were acquired with a Shimadzu UV2600 double beam spectrophotometer equipped with a ISR 2600 Plus integrating sphere. $BaSO_4$ was used as diffuse reflectance standard. The values of the band gaps were calculated from the diffuse reflectance spectra using the Tauc's plot for a direct gap transition.

2.2.3 | ICP-OES analyses

The Hf/(Hf+Zr) molar ratio of the solid solutions sample was determined by using an Agilent 5800 ICP-OES inductively coupled plasma-optical emission spectroscopy system. The samples were analyzed after dissolution in 4 M aqueous HCl.

2.2.4 | TG-DTA

Simultaneous TG-DTA measurements on samples of $BaZrS_3$ and $BaHfS_3$ were performed with a Netzsch STA 409 PC Luxx thermal analyzer. The measurements were performed in alumina crucibles under flowing Ar atmosphere (85 cm^3/min @STP, purity > 99.9995%) with a scan rate of 10 K/min in the range RT-1500°C.

2.2.5 | Raman spectroscopy

Raman spectra were acquired at room temperature using a Renishaw inVia Reflex Raman Microscope in a backscattering geometry. Raman spectra of $BaZrS_3$ and $BaHfS_3$ powder samples, which were sticked to double-sided carbon tapes, were measured with a 50× objective with the excitation wavelengths of 633 and 532 nm, respectively, in both cases with a spectral resolution of 0.5 cm^{-1}. In order to ensure that there was no laser damage on the samples, they were visually inspected before and after each measurement. Using a Si reference wafer, excitation lasers were calibrated.

3 | RESULTS AND DISCUSSION

The nominal compositions prepared were $BaZrS_3$, $BaHf_{0.25}Zr_{0.75}S_3$, $BaHf_{0.5}Zr_{0.5}S_3$, $BaHf_{0.75}Zr_{0.25}S_3$, and $BaHfS_3$. Most of the samples did not require any purification, as they were not appreciably contaminated by excess sulfur because during the rapid cooling of the samples once taken out of the furnace, sulfur vapors condensed on the walls of the glass ampules. In the few cases where free sulfur was detected in the samples by X-Ray diffraction (XRD) analysis, they were stirred for 1 h in hot (85°C) toluene, in which sulfur is fairly soluble,[23] then filtered and dried. After this treatment, no free elemental sulfur was detected in the samples. Toluene was chosen as a safer and much less toxic alternative to CS_2, which is the most common solvent used for dissolving elemental sulfur.

In all cases, the phase composition of the samples was analyzed by powder X-ray diffraction and, for the solid solutions, the agreement between the nominal and the actual composition was verified by ICP-OES analysis, as reported in Table 1.

The X-ray diffraction patterns (Figures S1–S5 in the Supporting Information) in all cases show only one phase in which the peaks positions and relative intensities gradually change from those of $BaZrS_3$ to those of $BaHfS_3$, which are isostructural (orthorhombic, space group Pnma, number 62, ICSD code 23288 for $BaZrS_3$, ICSD code 615918 for $BaHfS_3$) with $BaHfS_3$ possessing slightly smaller unit cell parameters compared to $BaZrS_3$. The gradual change of lattice parameters with increasing Hf/Zr ratio is clearly demonstrated in Figure 1 in which the position of the most intense XRD reflection, the (121) is displayed for all the compositions synthesized.

TABLE 1 Nominal compositions on solid solution samples (left column) versus actual compositions (right column) obtained from inductively coupled plasma-optical emission spectroscopy (ICP-OES) analyses.

Nominal composition	Actual composition
$BaHf_{0.75}Zr_{0.25}S_3$	$BaHf_{0.62\pm0.09}Zr_{0.38\pm0.08}S_3$
$BaHf_{0.5}Zr_{0.5}S_3$	$BaHf_{0.45\pm0.08}Zr_{0.5\pm0.1}S_3$
$BaHf_{0.25}Zr_{0.75}S_3$	$BaHf_{0.29\pm0.05}Zr_{0.7\pm0.1}S_3$

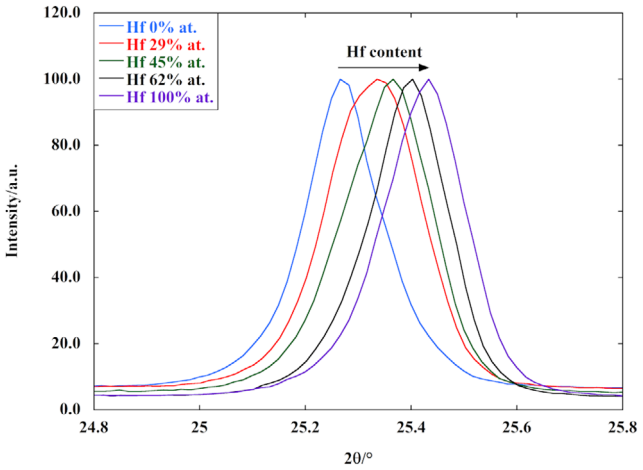

FIGURE 1 The (121) diffraction peak position (normalized intensities) as a function of Hf/(Hf+Zr) ratio.

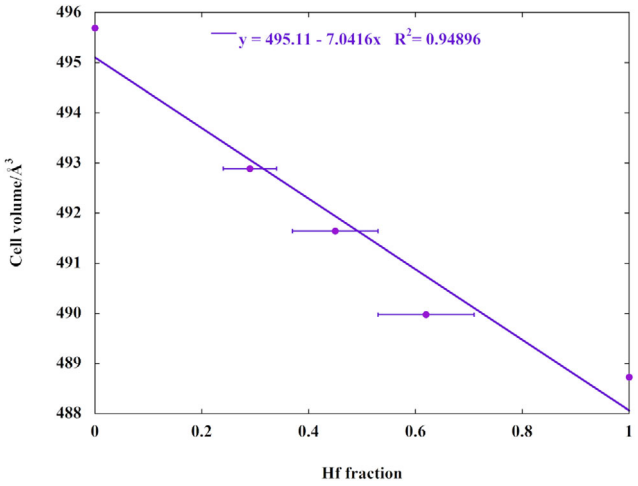

FIGURE 2 Unit cell volume of $BaHf_{1-x}Zr_xS_3$ compounds as a function of the Hf molar fraction.

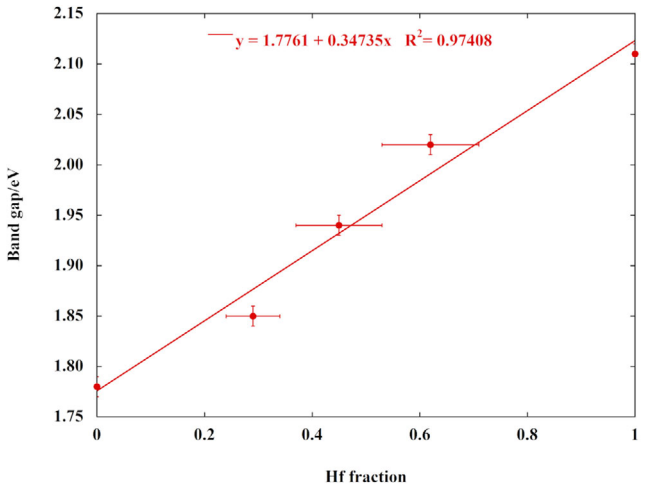

FIGURE 4 Band gap values of $BaHf_{1-x}Zr_xS_3$ as a function of Hf molar fraction.

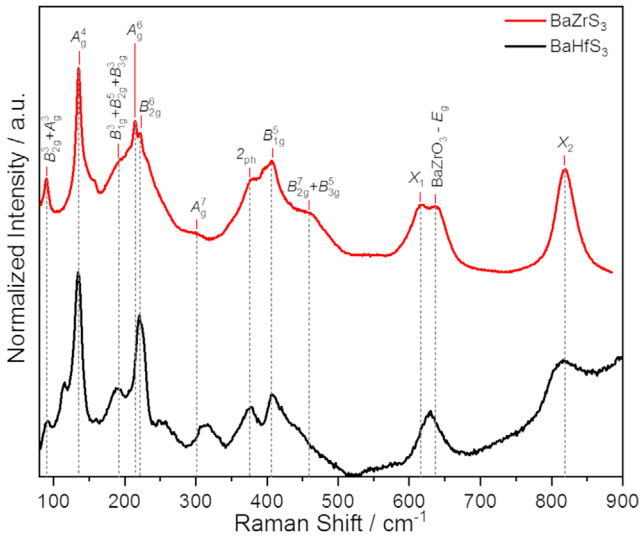

FIGURE 3 Raman spectrum of $BaZrS_3$ and $BaHfS_3$ measured with an excitation wavelength of 633 and 532 nm, respectively. The peak assignments for $BaZrS_3$ follow reference.[25]

All the diffraction patterns were analyzed by the Rietveld refinement procedure[24] in order to calculate the lattice parameters as a function of the composition. The cif file of $BaZrS_3$ was used for the refinement of the structure of the solid solutions by partly replacing Zr with the proper amount of Hf in the structure. The cell volume was found to change linearly with the Hf/(Hf+Zr) molar ratio, as demonstrated by Figure 2.

The Raman spectra of pure $BaZrS_3$ and pure $BaHfS_3$ are shown in Figure 3. The observed peaks in the Raman spectrum of $BaZrS_3$ match the literature and are assigned with individual modes according to Pandey et al.[25] Based on their calculations, the main contributions in the low frequency modes (<100 cm^{-1}) are stemming from the vibration of the Ba atoms, whereas the S atoms are mainly responsible for the high frequency phonons (>250 cm^{-1}).[25] In between, the mid-frequency modes are dominated by both Zr and S atoms. Notably, the Raman spectrum of $BaHfS_3$ exhibits similar peak intensities and positions. However, we observe a higher signal to noise for $BaHfS_3$ compared to $BaZrS_3$ when using a shorter wavelength excitation source presumably due to its higher band gap (see below), and some peaks appear better resolved. Since there appears to be no reliable reference Raman spectrum for $BaHfS_3$ in the literature and Raman spectra from various spots show no deviations, along with the single-phase Rietveld refinement analysis, we suppose that the $BaHfS_3$ Raman spectra can be used as a reference for future works.

Returning to the solid solution series, the effect of the substitution of Zr with Hf in the structure is also evident by looking at the color of the powders, which changes gradually from the dull black of $BaZrS_3$ to the orange-red of $BaHfS_3$, with the compounds that display a brownish-red hue that becomes more evident as the Hf content increases (Figures S6–S10 of the Supporting Information).

The shift in color is due to the enlargement of the band gap that increases linearly with increasing Hf content, as clearly shown in Figure 4.

The band gap value of each synthesized compound was obtained by using the Tauc's plot (direct band gap[26]) on their UV-Vis diffuse reflectance spectra, as shown in Figures S11–S15 of the Supporting Information.

X-ray diffraction and UV-Vis data demonstrate that it is possible to vary the crystal structure parameters and the band gap linearly with the Hf/(Hf+Zr) molar ratio. Furthermore, X-ray diffraction measurements show complete reciprocal solubility between $BaZrS_3$ and $BaHfS_3$, although this is not surprising, because Zr and Hf are the

most similar elements in the periodic table, being in the same group and possessing nearly identical atomic and ionic radii.[27,28] The cation substitution approach in $BaZrS_3$ to modify the gap of the material is not new, with studies in literature concerning, for example, Sr replacement of Ba[21] (though no solid solutions were prepared) and partial substitution of Zr with Ti, albeit with limited success,[6,26] because the mutual solubility range of $BaZrS_3$ and $BaTiS_3$ is very narrow and the $BaZrS_3$ perovskite structure is retained up to a Zr substitution of 7.5% by Ti. With higher Ti amounts, phase separation occurs.[26] For the first time, to the best of authors' knowledge, this work demonstrates the complete miscibility of $BaZrS_3$ and $BaHfS_3$ with the retention of perovskite structure common to both end members and its potential for a modulation of the band gap value of the prepared materials in a range of ~0.3 eV.

We think that the synthetic approach presented in this work is particularly effective because of three concurring factors. The first factor to be taken into account is the high exothermicity of the formation reactions of ZrS_2 and HfS_2 ($\Delta_f H^{\emptyset}_{773}$ (ZrS_2) = −592 kJ/mol[29] and $\Delta_f H^{\emptyset}_{773}$ (HfS_2) = −590 kJ/mol[30]). The heat evolved by the reaction of Zr(Hf) and S activates the reaction between BaS and excess sulfur (second factor) to form BaS_3 (third factor) that was proposed recently as a key intermediate in the formation of $BaZrS_3$ at temperatures near 500°C in a liquid-assisted reaction mechanism.[31] As a matter of fact, we confirm the previous report here, with the complete conversion of BaS to BaS_3 in presence of the same excess sulfur that we used for the ternary compounds, when heated together at 500°C for 6 days in evacuated sealed ampule. We performed the heating for a such long time to be sure to reach the equilibrium, but it is reasonable to assume that in presence of extra energy such that produced by the formation of ZrS_2 and HfS_2 the reaction between BaS and S may be very rapid. The diffraction pattern of the prepared BaS_3 is shown in Figure S16 of the Supporting Information. What we found agrees with literature results.[31]

Prolonging the reaction time does not affect appreciably the crystallinity of the reaction products. As an example, in Figure S17 of the Supporting Information, a comparison of the diffraction patterns of two samples of $BaZrS_3$, one obtained after an overnight thermal treatment and one after 6 days of thermal treatment (obviously both at 500°C) is shown. No relevant differences between the diffraction patterns are evident, both samples being phase pure and with peak positions, relative intensities and peak widths that do not show appreciable differences.

During our studies, also the effect of $BaCl_2$, widely used in literature as catalyst[19,20,31] was evaluated, preparing two samples of $BaZrS_3$, and adding in one of them an amount of $BaCl_2$ in a molar ratio $BaCl_2$/BaS 1:10, as proposed in literature.[19,20] The samples underwent the same thermal treatment at 500°C for 6 days, but no difference emerged from their X-ray diffraction patterns, as shown in Figure S18 of the Supporting Information. Due to the fact that $BaCl_2$ as a catalyst is not necessarily needed for the formation of $BaZrS_3$, having less materials in the reaction system simplifies the synthesis procedures, including purifying the final products and reducing the production of waste materials.

Finally, we investigated the thermal behaviour of the end members ($BaZrS_3$ and $BaHfS_3$) in inert (argon) atmosphere from room temperature to 1500°C by TG-DTA analyses. The thermograms (Figures S19 and S20 of the Supporting Information) demonstrate the refractory nature of the materials. Both materials show modest mass losses presumably due to sulfur vaporization (4.1% loss, Figure S19 for $BaZrS_3$, 1.5%, Figure S20 for $BaHfS_3$). No melting occurred in both cases, and one small thermal event due to a phase transition around 900°C was observed in the DTA profile of $BaZrS_3$, in agreement with literature data,[32] while no thermal events were observed in the DTA profile of $BaHfS_3$.

4 | CONCLUSIONS

In this paper, a simple and relatively fast synthetic approach was presented for the ceramic semiconductors $BaZrS_3$, $BaHfS_3$ and to their solid solutions, which are here demonstrated for the first time. $BaZrS_3$ and $BaHfS_3$ appear to be completely miscible in all ratios, and their unit cell volumes and band gap values vary both linearly with the composition. By varying the composition of the solid solutions, it is possible to modulate the band gap of the prepared materials in a range of ca. 0.3 eV. The modulability of the optoelectronic properties of these ceramic semiconductor materials, coupled with their remarkable physical and chemical stability, makes them intriguing alternatives to hybrid metal halide perovskites for applications in photovoltaic modules and other devices.

ACKNOWLEDGMENTS

The work of A.C. and A.L. was supported by Sapienza Università di Roma (grant number: RM12117A8484C2E0, Title: Stabilità termodinamica e cinetica di perovskiti ibride "lead-free" per applicazioni fotovoltaiche).

ORCID

Andrea Ciccioli https://orcid.org/0000-0003-1421-8062
Phillip J. Dale https://orcid.org/0000-0003-4821-8669
Alessandro Latini https://orcid.org/0000-0002-3205-4826

REFERENCES

1. Swarnka A, Mir WJ, Chakraborty R, Jagadeeswararao M, Sheikh T, Nag A. Are chalcogenide perovskites an emerging class of semiconductors for optoelectronic properties and solar cell? Chem Mater. 2019;31:565–75.
2. Sun YY, Agiorgousis ML, Zhang P, Zhang S. Chalcogenide perovskites for photovoltaics. Nano Lett. 2015;15:581–85.
3. Nishigaki Y, Nagai T, Nishiwaki M, Aizawa T, Kozawa M, Hanzawa K, et al. Extraordinary strong band-edge absorption in distorted chalcogenide perovskites. Sol. RRL. 2020;4:1900555.
4. Crovetto A, Nielsen R, Pandey M, Watts L, Labram JG, Geisler M, et al. Shining light on sulfide perovskites: $LaYS_3$ material properties and solar cells. Chem Mater. 2019;31:3359–69.
5. Kuhar K, Crovetto A, Pandey M, Thygesen KS, Seger B, Vesborg P, et al. Sulfide perovskites for solar energy conversion applications: computational screening and synthesis of the selected compound $LaYS_3$. Energy Environ Sci. 2017;10:2579–93.
6. Meng W, Saparov B, Hong F, Wang J, Mitzi DB, Yan Y. Alloying and defect control within chalcogenide perovskites for optimized photovoltaic application. Chem Mater. 2016;28:821–29.
7. Brunetti B, Cavallo C, Ciccioli A, Gigli G, Latini A. On the thermal and thermodynamic (In)stability of methylammonium lead halide perovskites. Sci Rep. 2016;6:31896.
8. Panetta R, Righini G, Colapietro M, Barba L, Tedeschi D, Polimeni A, et al. Azetidinium lead iodide: synthesis, structural and physico-chemical characterization. J Mater Chem A. 2018;6:10135–48.
9. Latini A, Gigli G, Ciccioli A. A study on the nature of the thermal decomposition of methylammonium lead iodide perovskite, $CH_3NH_3PbI_3$: an attempt to rationalise contradictory experimental results. Sustain Energy Fuels. 2017;1:1351–57.
10. Ciccioli A, Latini A. Thermodynamics and the intrinsic stability of lead halide perovskites $CH_3NH_3PbX_3$. J Phys Chem Lett. 2018;9:3756–65.
11. Ciccioli A, Panetta R, Luongo A, Brunetti B, Vecchio Ciprioti S, Mele ML, et al. Stabilizing lead halide perovskites with quaternary ammonium cations: the case of tetramethylammonium lead iodide. Phys Chem Chem Phys. 2019;21:24768–77.
12. Luongo A, Brunetti B, Vecchio Ciprioti S, Ciccioli A, Latini A. Thermodynamic and kinetic aspects of formamidinium lead iodide thermal decomposition. J Phys Chem C. 2021;125:21851–61.
13. Di Girolamo D, Phung N, Utama Kosasih F, Di Giacomo F, Matteocci F, Smith JA, et al. Ion migration-induced amorphization and phase segregation as a degradation mechanism in planar perovskite solar cells. Adv Energy Mater. 2020;10:2000310.
14. Vincent KC, Agarwal S, Turnley JW, Agrawal R. Liquid flux–assisted mechanism for modest temperature synthesis of large-grain $BaZrS_3$ and $BaHfS_3$ chalcogenide perovskites. Adv Energy Sustainability Res. 2023;4:2300010.
15. Turnley JW, Vincent KC, Pradhan AA, Panicker I, Swope R, Uible MC, et al. Solution deposition for chalcogenide perovskites: a low-temperature route to $BaMS_3$ materials (M = Ti, Zr, Hf). J Am Chem Soc. 2022;144;18234–39.
16. Clearfield A. The synthesis and crystal structures of some alkaline earth titanium and zirconium sulfides. Acta Cryst. 1963;16:135–42.
17. Lelieveld R, Ijdo DJW. Sulphides with the $GdFeO_3$ structure. Acta Cryst B. 1980;36:2223–26.
18. Nitta T, Nagase K, Hayakawa S. Formation, microstructure, and properties of barium zirconium sulfide ceramics. J Am Ceram Soc. 1970;53:601–4.
19. Wang Y, Sato N, Yamada K, Fujino T. Synthesis of $BaZrS_3$ in the presence of excess sulfur. J Alloys Compd. 2000;311:214–23.
20. Wang Y, Sato N, Fujino T. Synthesis of $BaZrS_3$ by short time reaction at lower temperatures. J Alloys Compd. 2001;327:104–12.
21. Niu S, Huyan H, Liu Y, Yeung M, Ye K, Blankemeier L, et al. Bandgap control via structural and chemical tuning of transition metal perovskite chalcogenides. Adv Mater. 2017;29:1604733.
22. Zilevu D, Parks OO, Creutz SE. Solution-phase synthesis of the chalcogenide perovskite barium zirconium sulfide as colloidal nanomaterial. Chem Commun. 2022;58:10512–15.
23. Jay S, Cézac P, Serin JP, Contamine F, Martin C, Mercadier J. Solubility of elemental sulfur in toluene between (267.15 and 313.15) K under atmospheric pressure. J Chem Eng Data. 2009;54:3238–41.
24. Lutterotti L, Chateigner D, Ferrari S, Ricote J. Texture, residual stress and structural analysis of thin films using a combined X-Ray analysis. Thin Solid Films. 2004;450:34–41.
25. Pandey J, Ghoshal D, Dey D, Gupta T, Taraphder A, Koratkar N, et al. Local ferroelectric polarization in antiferroelectric chalcogenide perovskite $BaZrS_3$ thin films. Phys Rev B. 2020;102:205308.
26. Wei X, Hui H, Perera S, Sheng A, Watson DF, Sun YY, et al. Ti-Alloying of $BaZrS_3$ chalcogenide perovskite for photovoltaics. ACS Omega. 2020;5:18579–83.
27. Slater JC. Atomic radii in crystals. J Chem Phys. 1964;41:3199–204.
28. Shannon RD. Revised effective ionic radii and systematic studies of interatomic distances in halides and chalcogenides. Acta Cryst. A. 1976;32:751–67.
29. Belov GV, Iorish VS, Yungman VS. IVTANTHERMO for Windows; database of thermodynamic properties of individual substances and thermodynamic modeling software, version 3.0. Moscow, Russia: Glushko Thermocenter of Russian Academy of Sciences; 2005.
30. Fiechter S, Eckert K. Crystal growth of HfS_2 by chemical vapour transport with halogen (Cl, Br, I). J Cryst Growth. 1988;88:435–41.
31. Yang R, Nelson J, Fai C, Arif Yetkin H, Werner C, Tervil M, et al. A low-temperature growth mechanism for chalcogenide perovskites. Chem Mater. 2023;35:4743–50.
32. Aslanov LA, Kovba LM. Ternary sulphides of barium and tantalum, titanium, zirconium. Russ J Inorg Chem. 1964;9:1317–19.

SUPPORTING INFORMATION

Additional supporting information can be found online in the Supporting Information section at the end of this article.

How to cite this article: Romagnoli L, Ciccioli A, Dale PJ, Yetkin HA, Panetta R, Latini A. A simple synthetic approach to $BaZrS_3$, $BaHfS_3$, and their solid solutions. J Am Ceram Soc. 2024;107:698–703. https://doi.org/10.1111/jace.19506